

## Two-dimensional Green's function and local density of states in photonic crystals consisting of a finite number of cylinders of infinite length

A. A. Asatryan,<sup>1</sup> K. Busch,<sup>2</sup> R. C. McPhedran,<sup>1</sup> L. C. Botten,<sup>3</sup> C. Martijn de Sterke,<sup>1</sup> and N. A. Nicorovici<sup>1</sup>

<sup>1</sup>*School of Physics, University of Sydney, Sydney, NSW 2006, Australia*

<sup>2</sup>*Institut für Theorie der Kondensierten Materie, University of Karlsruhe, P.O. Box 6980, 76128 Karlsruhe, Germany*

<sup>3</sup>*School of Mathematical Sciences, University of Technology, Sydney, NSW 2007, Australia*

(Received 27 June 2000; revised manuscript received 24 October 2000; published 29 March 2001)

Using the exact theory of multipole expansions, we construct the two-dimensional Green's function for photonic crystals, consisting of a finite number of circular cylinders of infinite length. From this Green's function, we compute the local density of states (LDOS), showing how the photonic crystal affects the radiation properties of an infinite fluorescent line source embedded in it. For frequencies within the photonic band gap of the infinite crystal, the LDOS decreases exponentially inside the crystal; within the bands, we find "hot" and "cold" spots. Our method can be extended to three dimensions as well as to treating disorder and represents an important and efficient tool for the design of photonic crystal devices.

DOI: 10.1103/PhysRevE.63.046612

PACS number(s): 42.70.Qs, 41.20.Jb, 42.25.Bs, 42.25.Fx

Photonic crystals, proposed by Yablonovitch [1] and John [2], are now a very active area of research [3–5] with the capacity for significant impact both in fundamental science and applications. In these materials, periodic dielectric constant variations prohibit the propagation of light in certain directions for certain bands of frequencies, thus allowing far-reaching control over the radiation dynamics of active materials embedded in them. Applications of photonic crystals include microscopic lasers [6], resonant antennas [7], optical fibers with photonic crystal cores [8], and optical switches [9]. With such applications in mind, the recent successful realizations [10–15] of two- and three-dimensional photonic crystals in the near-infrared and visible represent key milestones on the road to an integrated photonics.

Even though both pioneering works [1,2] were concerned with changes to the density of states by the photonic crystal, to date both theoretical and experimental characterization of finite-sized structures have largely been concerned with analyzing transmittance and reflection spectra [4]. This, however, provides little insight into how a photonic crystal modifies the electromagnetic vacuum as envisaged by Yablonovitch [1] and John [2]. This modification is encapsulated by the spatially resolved or local density of states (LDOS), the key quantity determining the radiation dynamics of fluorescent sources in a photonic crystal [16–18]. In three dimensions, it quantifies the coupling of an atom with transition frequency  $\omega$  at position  $\mathbf{r}$  to the modes of the photonic crystal and thus describes, for instance, how the photonic crystal affects the atom's emission rate. For infinite structures, the LDOS vanishes inside a complete band gap, and thus an excited two-level atom with a corresponding transition frequency cannot decay. Rather, a bound photon-atom state is formed [19]. The LDOS was calculated before for only a few isolated positions in infinite three-dimensional photonic crystals [20–22] and for one-dimensional structures [23].

In this paper, we extend the exact formalism of multipole expansions [24–26] to construct the two-dimensional Green's function  $G(\mathbf{r}, \mathbf{r}_s; \omega)$  of finite-sized two-dimensional photonic crystals composed of circular cylinders of infinite

length. Such two-dimensional geometries have received much attention lately because of their light-guiding properties [27]. Multipole methods were previously used for transmission and reflection calculations, but never in situations where the source may be inside a scatterer, which is required for a complete characterization of the Green's function. We use the Green's function to calculate the LDOS,  $\rho(\mathbf{r}; \omega)$ , via [28,29]

$$\rho(\mathbf{r}; \omega) = -\frac{2\omega}{\pi c^2} \text{Im}[G(\mathbf{r}, \mathbf{r}; \omega)]. \quad (1)$$

Here,  $G(\mathbf{r}, \mathbf{r}_s; \omega)$  is the electromagnetic Green's function for a source at location  $\mathbf{r}_s$  and observation point at  $\mathbf{r}$ . The source, a line antenna of infinite length parallel to the cylinder axes, radiates with harmonic time dependence  $\exp(-i\omega t)$ . We note that in vacuum,  $[2\omega/(\pi c^2)]^{-1} \rho(\mathbf{r}; \omega) = 0.25$ . The clusters that we consider have features that differ from the corresponding infinite structure. For instance, for frequencies inside the photonic band gap of the infinite structure and locations deep inside the cluster, the LDOS is small but does not vanish [see Figs. 1(a) and 2(a)]. Additional features appear closer to the cluster surface.

The clusters we consider consist of  $N_c$  parallel, nonoverlapping dielectric cylinders with radii  $a_l$  and refractive indices  $n_l$  centered at positions  $\mathbf{c}_l$  in a medium with refractive index  $n_b = 1$ . For propagation perpendicular to the cylinder axes, which is the only direction that needs to be considered in a two-dimensional problem, the polarizations of the electromagnetic waves decouple. The problem can then be specified by a single field component  $G$ , i.e.,  $G = E_z$  (TM polarization) and  $G = H_z$  (TE polarization), when the electric and magnetic fields are polarized parallel to the cylinder axes, respectively. Here we only consider TM polarization, the derivation for TE polarization being similar. The Green's function  $G$  satisfies the wave equation

$$\nabla^2 G + k^2 n^2(\mathbf{r}) G = \delta(\mathbf{r} - \mathbf{r}_s) \quad (2)$$

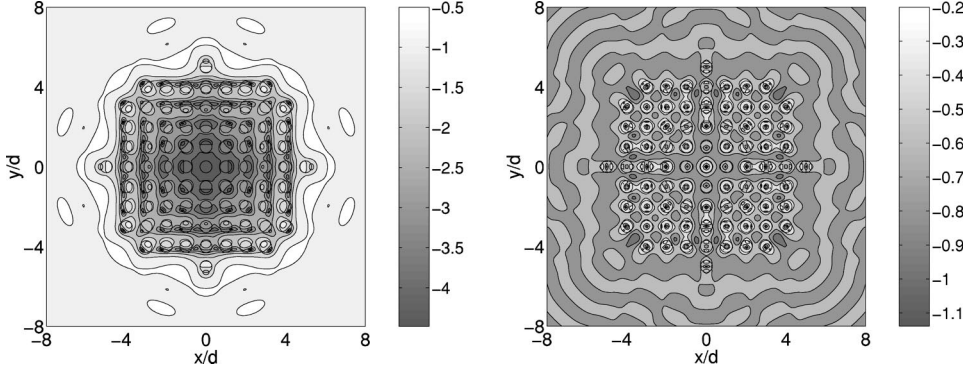


FIG. 1. Contour plot of  $\log_{10}(\rho\pi c^2/2\omega)$  versus position, using a logarithmic scale. (a)  $\lambda/d = 3.5$ , in the low-transmission region; (b)  $\lambda/d = 2.5$ , in the high-transmission region.

together with the boundary conditions that at the surface of each cylinder,  $G$  and its normal derivative  $\partial G/\partial n$  are continuous.

In the vicinity of the  $l$ th cylinder and using *local coordinates*  $r_l$ ,  $\theta_l$  to facilitate imposition of boundary conditions, the Green's function  $G$  can be written as

$$G(\mathbf{r}_l) = \sum_{m=-\infty}^{\infty} [A_m^l J_m(kr_l) + B_m^l H_m^{(1)}(kr_l)] e^{im\theta_l}, \quad (3)$$

while inside the cylinder it may be expanded as

$$G(\mathbf{r}_l) = \sum_{m=-\infty}^{\infty} C_m^l J_m(kr_l) e^{im\theta_l}, \quad (4)$$

where  $A_m^l$ ,  $B_m^l$ , and  $C_m^l$  depend on the source position. Here,  $J_m$  and  $H_m^{(1)}$  are Bessel and outgoing Hankel functions of order  $m$ , respectively. By imposing the boundary conditions on the surface of each cylinder, we express the coefficients  $A_m^l$  and  $C_m^l$  in terms of the  $B_m^l$ .

Applying now Green's theorem over the total structure, and using Sommerfeld's radiation condition at infinity, together with the subsequent application of Graf's addition theorem, we derive a partitioned system of linear equations in the modal coefficients  $B_m^l$  ( $l = 1, 2, \dots, N_c$ ),

$$M_p^l B_p^l + \sum_{q=1}^{N_c} \sum_{m=-\infty}^{\infty} H_{p-m}^{(1)}(kr_{lq}) e^{i(m-p)\theta_{lq}} B_m^q = K_p^l, \quad (5)$$

where the first sum excludes the term  $q=l$ , and  $M_p^l$  is

$$M_p^l = \frac{n_l J_p'(n_l k a_l) H_p^{(1)}(k a_l) - J_p(n_l k a_l) H_p^{(1)'}(k a_l)}{n_l J_p'(n_l k a_l) J_p(k a_l) - J_p(n_l k a_l) J_p'(k a_l)}. \quad (6)$$

Here,  $r_{lq}$  is the distance between the centers of cylinders  $l$  and  $q$ , and  $\theta_{lq}$  is the argument of  $\mathbf{r}_{lq} \equiv \mathbf{r}_q - \mathbf{r}_l$ . Finally, primes denote differentiation with respect to the argument. The source contribution  $K_p^l$  in Eq. (5) is

$$K_p^l = -\frac{1}{4i} H_p^{(1)}(k r_{ls}) e^{-ip\theta_{ls}} \quad (7)$$

when the source is in the background medium, and

$$K_p^l = -\frac{J_p(k n_l r_{ls}) e^{-ip\theta_{ls}} / (2\pi k a_l)}{n_l J_p'(n_l k a_l) J_p(k a_l) - J_p(n_l k a_l) J_p'(k a_l)} \quad (8)$$

when the source is inside cylinder  $l$ . Finally,  $K_p^l = 0$  when the source is inside any of the cylinders  $q \neq l$ .

Solving the inhomogeneous linear set (5) for the multipole coefficients  $B_m^l$  allows us to construct the Green's function of the cluster. Five different cases need to be distinguished. First, when  $\mathbf{r}$  and  $\mathbf{r}_s$  are in the same cylinder,

$$G(\mathbf{r}, \mathbf{r}_s) = G_0(\mathbf{r}, \mathbf{r}_s) + \sum_{m=-\infty}^{\infty} C_m^l J_m(k n_l r_l) e^{im\theta_l}, \quad (9)$$

where  $G_0 = H_0^{(1)}(k n_l |\mathbf{r} - \mathbf{r}_s|) / (4i)$  is the Green's function for a homogeneous medium with refractive index  $n_l$ . If  $\mathbf{r}$  and  $\mathbf{r}_s$  are in different cylinders, or if  $\mathbf{r}$  is in one of the cylinders, and  $\mathbf{r}_s$  is in the background medium, then  $G$  is given by Eq. (9), but without the  $G_0$  term. In contrast, if both  $\mathbf{r}$  and  $\mathbf{r}_s$  are in the background medium, then

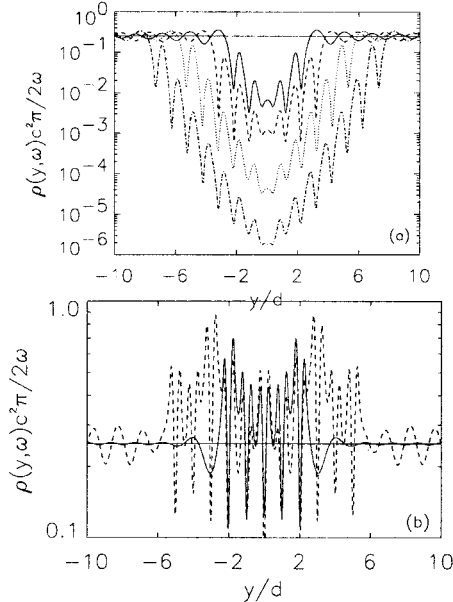


FIG. 2. Sections through Fig. 1 at  $x=0$ . (a)  $\lambda/d = 3.5$  and  $N_c = 21, 45, 81$ , and  $149$  (top to bottom); (b)  $\lambda/d = 2.5$  and  $N_c = 21$  (solid line) and  $81$  (dashed line).

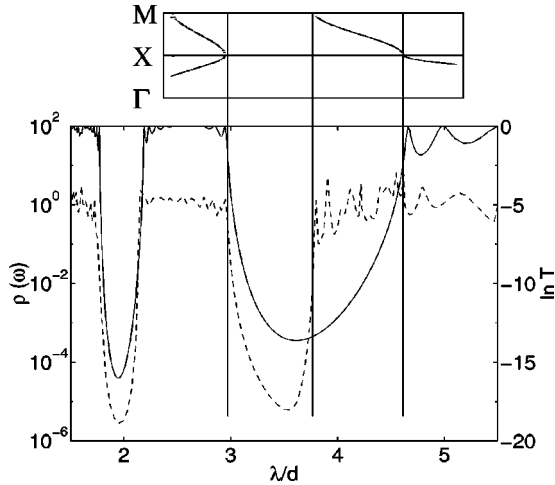


FIG. 3. Solid line: Normal incidence transmissivity of a 10-layer-thick stack of cylinders, with parameters given in the text, versus wavelength (right-hand scale). Dashed line:  $[2\omega/(\pi c^2)]^{-1}\rho(\omega)$  versus  $\lambda$  in the central cell for  $N_c=149$ . The inset shows a part of the band diagram for the infinite structure on  $\Gamma$ - $X$ - $M$ . The vertical lines are included to aid the eye.

$$G(\mathbf{r}, \mathbf{r}_s) = G_0(\mathbf{r}, \mathbf{r}_s) + \sum_{l=1}^{N_c} \sum_{m=-\infty}^{\infty} B_m^l H_m^{(1)}(kr_l) e^{im\theta_l}, \quad (10)$$

with  $n_l$  in  $G_0$  replaced by unity. Finally, if the source  $\mathbf{r}_s$  is situated in one of the cylinders and  $\mathbf{r}$  is in the background medium, then  $G$  is given by Eq. (10) without the  $G_0$  term.

We take all cylinders to have the same radius  $a$  and refractive index  $n_c=3$ . The cylinders are arranged in a square lattice with period  $d$ , and  $a/d=0.3$ , corresponding to an area fraction of 28.3%. The dashed line in Fig. 3 shows the normal incidence transmission through such a structure that has a thickness of  $10d$  and infinite transverse dimension [30,31]. It shows two low-transmission regions for  $3 < \lambda/d < 5$  and  $1.8 < \lambda/d < 2.1$ .

The clusters for which we calculate the LDOS are constructed hierarchically by adding shells to a central cylinder such that the emerging structure comprises a finite-sized section of a two-dimensional photonic crystal. Since the cylinders in each shell have the same distance to the cluster's center, as the size increases, the cluster acquires an approximately circular form.

The accuracy of solutions (9) and (10), describing the field inside and outside the cylinders, respectively, is governed by the highest order of circular harmonics  $N$  that is retained. It can be tested by checking the degree to which the boundary conditions on the cylinder surfaces are satisfied. As an example, at a wavelength  $\lambda/d=3.5$  and for a cluster of 45 cylinders, the boundary conditions were satisfied with a relative accuracy of better than  $10^{-7}$  for  $N=10$ . We also checked the reciprocity condition  $G(\mathbf{r}, \mathbf{r}_s) = G(\mathbf{r}_s, \mathbf{r})$  for various field and source points and achieved a relative accuracy of  $10^{-10}$ . Thus, by using sufficient multipole coefficients, the Green's function can be found to any desired accuracy. All calculations below have relative accuracy better than  $10^{-4}$ . It

is important to note from Eq. (5) that, for a given frequency, the source coefficients  $B_p^l$ , which constitute the complete solution, may be found from a single matrix inversion; our method is therefore computationally very efficient.

Figure 1 shows  $\pi c^2 \rho(\mathbf{r}; \omega)/(2\omega)$ , for a cluster with  $N_c=81$ , for  $\lambda/d=3.5$  near the center of the first low-transmission region [Fig. 1(a)], and  $\lambda/d=2.5$ , in the high-transmission region [Fig. 1(b)] (color versions of these figures are available at [www.physics.usyd.edu.au/~ara](http://www.physics.usyd.edu.au/~ara)). The black circles indicate the cylinder edges. From Fig. 1(a), we see that  $\rho(\mathbf{r}; \omega)$  within the low-transmission region is small everywhere in the interior of the structure, and that there is a boundary layer with a thickness of roughly a single lattice constant that separates the cluster's interior from the vacuum. A section of Fig. 1(a) at  $x=0$  is shown in Fig. 2(a), for  $N_c=21, 45, 81, 149$  for the same wavelength. Clearly, for a given cluster size, the LDOS decreases exponentially towards the center. In addition, the LDOS in the central cell decreases exponentially with cluster size. However, there are also strong regular variations of the LDOS within each cell. As we increase the cluster size, the positions of the minima and maxima exhibit no notable changes. Outside the cluster, the LDOS rapidly approaches its free space value of 0.25, indicated by the horizontal straight line. The LDOS reaches its lowest value at the central cylinder's edge, where  $\rho(\mathbf{r}; \omega) \approx 3.3 \times 10^{-5}$ , almost four orders of magnitude smaller than the vacuum value. Consequently, the emission of a line antenna located here is reduced by about four orders of magnitude. The low values for both the transmittance and the LDOS indicate the presence of a photonic band gap at  $\lambda/d=3.5$ .

Turning now to Fig. 1(b), for the high-transmission wavelength  $\lambda/d=2.5$  we see that  $\rho(\mathbf{r}; \omega)$  does not decrease strongly inside the structure and varies around the vacuum value of 0.25. Figure 2(b) gives again a section at  $x=0$  for  $N_c=21$  and 81. Inside the cluster, enhancements of as much as 3.5 over the vacuum value can be seen. The LDOS reaches its lowest value of 0.07 in the center of the central cell, almost three times lower than the vacuum level. Similar suppression effects have been obtained for infinite crystals [20,21].

Finally, we define the total density of states (DOS)  $\rho(\omega)$  to be the weighted average of the LDOS over the Wigner-Seitz cell (WSC), i.e.,

$$\rho(\omega) = \frac{1}{d^2} \int_{\text{WSC}} \varepsilon(\mathbf{r}) \rho(\mathbf{r}; \omega) d\mathbf{r}. \quad (11)$$

In Fig. 3, we plot  $\rho(\omega)$  in the central Wigner-Seitz cell for  $N_c=149$  (dashed line). Note the correlation between this curve and the transmission data (solid line)—high transmission corresponding to a large density of states. However, the opposite is not true in general. Though the low-transmission regions  $1.8 < \lambda/d < 2.1$  and  $3.0 < \lambda/d < 3.8$  correspond to a low density of states, for  $3.8 < \lambda/d < 5.0$  the transmission is low, yet the DOS is large.

The behavior for  $3.8 < \lambda/d < 5.0$  can be understood as follows. The transmission shown in Fig. 3 is for normal incidence, i.e., incidence in the  $X$  direction for an infinite struc-

ture. For non-normal incidence, the low-transmission region we are considering shifts to shorter wavelengths, indicating the presence of states that are not accessible at normal incidence, but that of course are included in the density of states. This argument can also be cast in the language of infinite media, though the finite structures we are dealing with make this somewhat hazardous: the normal incidence transmission only depends on the states in the  $\Gamma$ - $X$  section of the Brillouin zone. However, the LDOS and the DOS that we compute of course sample the entire Brillouin zone. Indeed, a calculation of the band structure on the Brillouin-zone edge between  $X$  and  $M$ , where  $M$  designates the zone corner, confirms the presence of states for  $3.8 < \lambda/d < 5.0$ . This is illustrated in the inset of Fig. 3, which shows the part of the band diagram of the infinite structure on  $\Gamma$ - $X$ - $M$ . It is also confirmed by results for non-normal transmission that are not shown here.

In conclusion, we have developed a robust method for calculating the LDOS of finite two-dimensional photonic crystals that is based on the exact theory of multipole expan-

sions. It is highly accurate and efficient, since a calculation requires only a single matrix inversion for a complete diagram such as Fig. 1. Thus, the large parameter space provided by these structures through possible locations and transition frequencies of active materials may be investigated efficiently. By spatial integration, we also obtain the total DOS for a finite structure. The method can also be applied to disordered structures as well as to structures with material dispersion. Further, though we have considered dielectrics only, the method is also applicable when  $n$  is complex, i.e., in the presence of gain or loss [32,33]. Finally, three-dimensional structures, which are of direct relevance to non-linear and quantum optical theories and experiments, can be treated similarly.

We thank P. Das for help in preparing the graphs. This work was supported by the Australian Research Council. K.B. acknowledges support by the Deutsche Forschungsgemeinschaft under Grant No. Bu 1107/2-1.

- 
- [1] E. Yablonovitch, Phys. Rev. Lett. **58**, 2059 (1987).
  - [2] S. John, Phys. Rev. Lett. **58**, 2486 (1987).
  - [3] J.D. Joannopoulos, R.D. Meade, and J.N. Winn, *Photonic Crystals: Molding the Flow of Light* (Princeton University Press, Princeton, NJ, 1995).
  - [4] *Photonic Band Gap Materials*, edited by C.M. Soukoulis, Vol. 315 of *NATO Advanced Study Institute Series E: Applied Sciences* (Kluwer, Dordrecht, 1996).
  - [5] Special issue on photonic crystals, J. Lightwave Technol. **17**(11) (1999).
  - [6] O. Painter, R.K. Lee, A. Scherer, A. Yariv, J.D. O'Brien, P.D. Dapkus, and I. Kim, Science **284**, 1819 (1999).
  - [7] B. Temelkuran, M. Bayindir, E. Ozbay, R. Biswas, M.M. Sigalas, G. Tuttle, and K.M. Ho, J. Appl. Phys. **87**, 603 (2000).
  - [8] J.C. Knight, J. Broeng, T.A. Birks, and P.St.J. Russel, Science **282**, 1476 (1998).
  - [9] K. Busch and S. John, Phys. Rev. Lett. **83**, 967 (1999).
  - [10] A. Birner *et al.*, Phys. Status Solidi A **165**, 111 (1998).
  - [11] J.E.G.J. Wijnhoven and W. Vos, Science **281**, 802 (1998).
  - [12] A.A. Zakhidov *et al.*, Science **282**, 897 (1998).
  - [13] S. Lin *et al.*, Nature (London) **394**, 251 (1998).
  - [14] S. Noda *et al.* (Ref. [5]), p. 1948.
  - [15] A. Blanco *et al.*, Nature (London) **405**, 437 (2000).
  - [16] S.W. Leonard *et al.*, Appl. Phys. Lett. **75**, 2063 (1999).
  - [17] R. Sprik, B.A. van Tiggelen, and A. Lagendijk, Europhys. Lett. **35**, 265 (1996).
  - [18] K. Busch, N. Vats, S. John, and B.C. Sanders, Phys. Rev. E **62**, 4251 (2000).
  - [19] S. John and J. Wang, Phys. Rev. Lett. **64**, 2418 (1990); Phys. Rev. B **43**, 12 772 (1991).
  - [20] K. Busch and S. John, Phys. Rev. E **58**, 3896 (1998).
  - [21] S. John and K. Busch (Ref. [5]), p. 1931.
  - [22] Z.-Y. Li, L.-L. Lin, and Z.-Q. Zhang, Phys. Rev. Lett. **84**, 4341 (2000).
  - [23] A. Moroz, Europhys. Lett. **46**, 419 (1999).
  - [24] V. Twersky, J. Acoust. Soc. Am. **24**, 42 (1952).
  - [25] D. Felbacq *et al.*, J. Opt. Soc. Am. A **11**, 2526 (1994).
  - [26] L.-M. Li and Z.-Q. Zhang, Phys. Rev. B **58**, 9587 (1998).
  - [27] A. Mekis, J.C. Chen, I. Kurland, S. Fan, P.R. Villeneuve, and J.D. Joannopoulos, Phys. Rev. Lett. **77**, 3787 (1996).
  - [28] E.N. Economou, *Green's Functions in Quantum Physics* (Springer-Verlag, Berlin, 1983).
  - [29] P. Sheng, *Introduction to Wave Scattering, Localization, and Mesoscopic Phenomena* (Academic Press, San Diego, 1995).
  - [30] A.A. Asatryan, P.A. Robinson, L.C. Botten, R.C. McPhedran, N.A. Nicorovici, and C. Martijn de Sterke, Phys. Rev. E **60**, 6118 (1999).
  - [31] A.A. Asatryan, P.A. Robinson, L.C. Botten, R.C. McPhedran, N.A. Nicorovici, and C. Martijn de Sterke, Phys. Rev. E **62**, 5711 (2000).
  - [32] A. Tip, Phys. Rev. A **57**, 4818 (1998).
  - [33] H. Cao, J.Y. Xu, D.Z. Zhang, S.-H. Chang, S.T. Ho, E.W. Seelig, X. Liu, and R.P.H. Chang, Phys. Rev. Lett. **84**, 5584 (2000).